2013 IEEE/RSJ International Conference on
Intelligent Robots and Systems (IROS)
November 3-7, 2013. Tokyo, Japan

Integrated Navigation System using Camera and Gimbaled Laser Scanner for Indoor and Outdoor Autonomous Flight of UAVs

Sungsik Huh, David Hyunchul Shim, and Jonghyuk Kim, *Member, IEEE*

Abstract— **This paper describes an integrated navigation sensor module, including a camera, a laser scanner, and an inertial sensor, for unmanned aerial vehicles (UAVs) to fly both indoors and outdoors. The camera and the gimbaled laser sensor work in a complementary manner to extract feature points from the environment around the vehicle. The features are processed using an online extended Kalman filter (EKF) in simultaneous localization and mapping (SLAM) algorithm to estimate the navigational states of the vehicle. In this paper, a new method is proposed for calibrating a camera and a gimbaled laser sensor. This calibration method uses a simple visual marker to calibrate the camera and the laser scanner with each other. We also propose a real-time navigation algorithm based on the EKF SLAM algorithm, which is suitable for our camera-laser sensor package. The algorithm merges image features with laser range data for state estimation. Finally, these sensors and algorithms are implemented on our octo-rotor UAV platform and the result shows that our onboard navigation module can provide a real-time three-dimensional navigation solution without any assumptions or prior information on the surroundings.**

I. Introduction

The Global Positioning System (GPS) is widely used for the localization of ground and aerial vehicles and provides a very accurate position measurement wherever available. Unmanned aerial vehicles have been very successful thanks to the advent of GPS in mid 1990s and there are growing interests to use them for indoor surveillance or mapping. Since GPS cannot be used indoor, alternative localization methods should be developed. Such methods will be very useful wherever GPS is not available due to obstruction or jamming. They can be also applied not only to UAVs but also ground vehicles and underwater vehicles operating in the environment where GPS is not reliable or unavailable. Such localization methods should be capable of full three-dimensional (3D) navigation in both unstructured indoor and outdoor environments.

The 3D navigation system is required to provide precise and instant pose estimation without prior information or assumptions on the characteristics of the environment, including depth. The system needs to include general algorithms for mapping and localization that work just about anywhere without any constraints. Map representations must be fully in 3D and capable of representing arbitrary 3D geometry at a level of resolution that is appropriate for the vehicle's navigation and its task.

In addition, the navigation system should be able to detect obstacles that are in the path of the vehicle. Thus, it is necessary to have the ability to create a dense environmental description, such as a grid map. A dense grid map, which is different from a sparse feature map, is necessary because the ability to distinguish between free and occupied space is essential for collision-free navigation and autonomous exploration in a multi-level environment.

Previous studies in [1][2][3] discuss the indoor navigation based on two-dimensional (2D) maps or multi-layered maps. However, in unstructured 3D environments, the assumptions from these studies are not always viable. In [4], a stereoscopic camera was used to generate a depth map of the area surrounding the vehicle and RGB-Depth (RGB-D) camera was used in [5]. However, the depth maps generated by these sensors have relatively short measurement ranges, which are useful for indoor navigation. Monoscopic cameras with downward-aimed, wide-angle lenses have been investigated in [6] and [7] for control of hovering, take-off, landing, and small-scale mapping, but they are hard to describe the rich information about the absolute value of depth and the forward view of the vehicle.

There is a comprehensive study on real-time localization with a laser scanner and an inertial measurement unit (IMU) [8] during aggressive maneuver in 3D environments using a Gaussian particle filter, but it requires an a priori known 3D octree grid map known *a priori*.

This paper proposes a navigation module with a camera and a gimbaled laser scanner that can estimate the pose of the vehicle and build a map in GPS-denied environments such as indoor or where GPS signal reception is poor or jammed. The two-dimensional laser scanner and camera have different characteristics for their sensing methods, ranges, and accuracies. Therefore, these different sensors can be combined so that they complement each other and give better measurements and state estimations from the environment around the vehicle.

In Section II, we first propose a new method for calibrating a camera with a laser scanner mounted on a tilting gimbal rotated by a servo motor with an embedded rotary encoder. After the calibration, the sensor module, which also includes an IMU, can measure the environment in its field of view and provide images, range data, and bearing data from point clouds.

*This research was supported by the National Research Foundation of Korea (NRF) funded by the Korean government (Ministry of Science, ICT & Future Planning) (No.2013042123)

S. Huh and D. H. Shim are with the Department of Aerospace Engineering, Korea Advanced Institute of Science and Technology (KAIST), Daejeon, Republic of Korea (phone: +82-42-350-3724; fax: +82-42-350-3710; e-mail: {hs2, hcshim}@kaist.ac.kr).

J. Kim is with the School of Engineering, Australian National University, ACT 0200, Australia (e-mail: jonghyuk.kim@anu.edu.au).

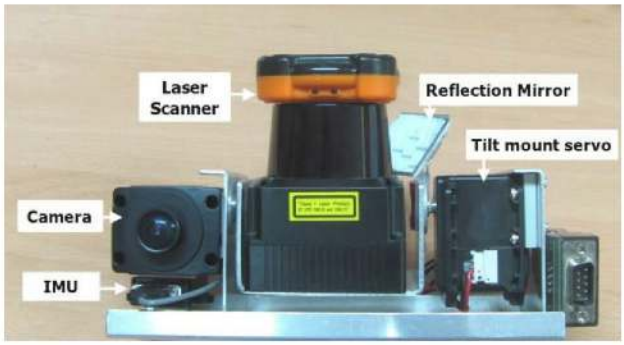

Figure 1. Camera-gimbaled laser sensor module prototype.

Section III provides detailed explanation for a navigation algorithm that the pose of the vehicle and landmarks are instantly estimated by a modified EKF SLAM based on the monocular-SLAM [9] framework. The proposed navigation algorithm is implemented on an octo-rotor type UAV platform equipped with the sensor module and a GPS receiver. Indoor and outdoor flight test results are shown and discussed in Section IV.

II. Camera and Gimbaled Laser Sensor Module

A. Sensor fusion

The sensor module consists of a fixed camera, a planar laser scanner mounted on a tilting gimbal rotated by a servo motor, and an inertial measurement unit as shown in Fig. 1. The laser scanner, which is mounted on the tilting gimbal, rotates and scans the 3D environment to acquire range and bearing data covering the field of view of the camera. The azimuth of the laser scanner is measured internally and its elevation (tilt angle) is measured by a rotary encoder attached to the servo motor. A laser reflection mirror is installed at a corner of the scanner to measure upward or downward distance. This mirror can reflect a portion of the laser scanning rays up or down from the gimbal mount.

B. Calibration of camera and gimbaled laser scanner

Before using the sensor module, the camera and the gimbaled laser scanner sensor should be mutually calibrated since imprecise relative pose between these sensors can cause large matching errors. Methods for calibration between a camera and a nodding laser scanner have already been developed such as [10]. However, we used a marker whose pattern is simpler than that of a chessboard, and applied a less laborious method which does not require one to select corner points.

A red, circular visual marker, as shown in Fig. 2, is used to calibrate the camera and gimbaled laser scanner. The calibration marker has a distinct color and is more protruded than other objects in the office so that simple detection algorithms can detect and label the marker for both the laser scanner and the camera. The biggest red blob can be detected as the relevant marker using a simple image processing algorithm and the closest 3D points captured by the laser scanner can be labeled using a distance threshold as depicted in Fig. 3.

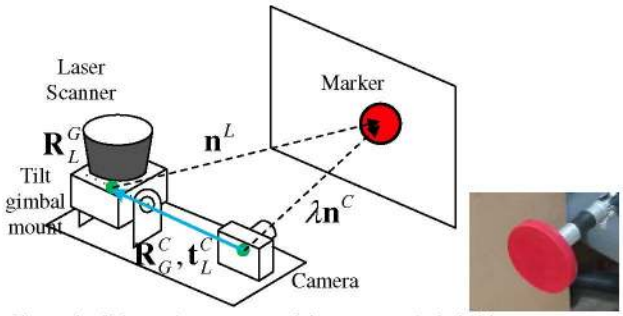

Figure 2. Schematic geometry of the camera-gimbaled laser scanner calibration method (left) and a picture of the visual marker (right).

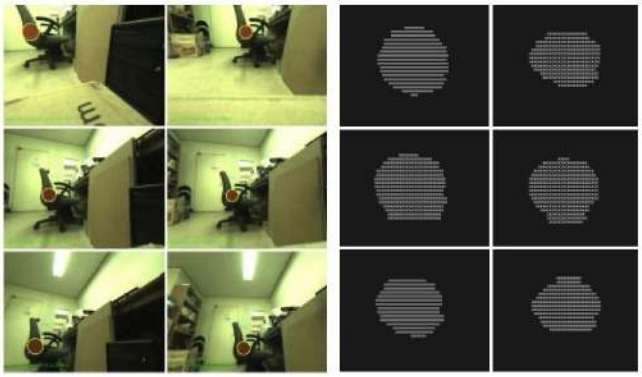

Figure 3. Marker detected images at different viewpoint of the sensor module (left) and labeled marker images by gimbaled laser scanner (right).

After the labeling of the bearing and range of the markers at different positions from the images and laser scanned 3D data, they are matched in order to calculate the disparity between them. We calculate the relative, three degrees of freedom (3-DOF) attitude between the two sensors since we can manually measure the relative translation between the two sensors in advance.

The vector equation between the two sensors and the marker is derived as:

$$\lambda\mathbf{n}^C = \mathbf{t}_L^C + \mathbf{R}_G^C\mathbf{R}_L^G\mathbf{n}^L \tag{1}$$

where $\mathbf{n}^C$ and $\mathbf{n}^L$ are a vector from the camera to the marker position in inertial coordinates and a vector from the laser scanner to the marker in inertial coordinates, respectively as:

$$\mathbf{n}^C = \begin{bmatrix} \cos z_\psi^C \cos z_\theta^C & \sin z_\psi^C & -\cos z_\psi^C \sin z_\theta^C \end{bmatrix}^T \tag{2}$$

$$\mathbf{n}^L = \begin{bmatrix} z_\rho^L \cos z_\psi^L & z_\rho^L \sin z_\psi^L & t_z^L \end{bmatrix}^T. \tag{3}$$

The origin of gimbal mount frame and the laser scanner frame is identical so that the rotation matrix from the laser coordinates to the center of the tilting gimbal mount $\mathbf{R}_L^G$ is given as:

$$\mathbf{R}_L^C = \mathbf{R}_G^C\mathbf{R}_L^G = \begin{bmatrix} R_{G00}^C & R_{G01}^C & R_{G02}^C \\ R_{G10}^C & R_{G11}^C & R_{G12}^C \\ R_{G20}^C & R_{G21}^C & R_{G22}^C \end{bmatrix} \begin{bmatrix} \cos\theta_G & 0 & \sin\theta_G \\ 0 & 1 & 0 \\ -\sin\theta_G & 0 & \cos\theta_G \end{bmatrix}. \tag{4}$$

In order to take the direct linear transformation (DLT) [11], the following equation and parameters can be

rearranged into "Aτ=b" matrix form. It is then possible to use the pseudo-inverse to solve the over-determined problem:

$$\tau = A^{+}b = A^{+}\left(\mathbf{t}_L^C + \lambda \mathbf{n}_i^C\right) \tag{5}$$

where the components of the equation are substituted with measured bearing and range data to the marker:

$$\tau=\left[R_{G00}^C \; R_{G01}^C \; R_{G02}^C \; R_{G10}^C \; R_{G11}^C \; R_{G12}^C \; R_{G20}^C \; R_{G21}^C \; R_{G22}^C\right]^T \tag{6}$$

$$A_{3n\times 9} = \begin{bmatrix} \mathbf{a} & \mathbf{0}_{1\times3} & \mathbf{0}_{1\times3} \\ \mathbf{0}_{1\times3} & \mathbf{a} & \mathbf{0}_{1\times3} \\ \mathbf{0}_{1\times3} & \mathbf{0}_{1\times3} & \mathbf{a} \\ & \vdots & \end{bmatrix} \tag{7}$$

$$\mathbf{a} = \begin{bmatrix} z_\rho^L \cos z_\psi^L \cos\theta_G + t_z^L \sin\theta_G \\ z_\rho^L \sin z_\psi^L \\ -z_\rho^L \cos z_\psi^L \sin\theta_G + t_z^L \cos\theta_G \end{bmatrix}^T. \tag{8}$$

More measurements without outliers yield more precise results. In addition, the relative 3-DOF attitude can be highly enhanced if an optimization method, such as Levenberg-Marquardt, is also applied using an initial value from the DLT calculation.

C. Feature detection and frame-to-frame matching

The amount of image and laser data that is available is too massive to use on a second-by-second basis, so it is necessary to efficiently extract useful data. We mainly use significant corner features and distinguishing points in an image.

First, features are detected in an image from the camera. We implemented the FAST feature detector [11] and the Shi-Tomasi feature detector [12], which provides eigenvalues and eigenvectors of points resulting from image-gradient calculations.

For frame-to-frame matching and tracking, the pyramidal image-based Lucas-Kanade optical tracker [13] is used. As features move in and out of the camera's field of view, our feature management algorithm removes vanishing features and registers emergent ones in a continuous sequence of images. The management algorithm allows up to 30 features, having higher eigenvalues, to be tracked, and it manages the distances between tracked features so that they are located sparsely.

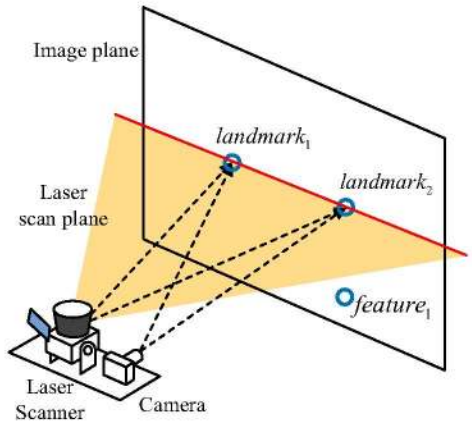

Figure 4. Schematic diagram: Conversion from features at different elevation angle to landmarks by the tilt mount and laser range data.

Laser range data are matched with features in the camera's field of view when a line-of-sight (LOS) towards a feature from the camera and the scanning plane of the laser intersect with each other. Since perfect line-plane matching rarely happens in reality, we set an angular threshold between the line and the plane considering the resolution of the rotary encoder. Once the line and the laser plane intersect, the closest laser measurement to the LOS of the camera is chosen for matching. Laser range data is added to the matched feature for undelayed range estimation and the feature is registered immediately as a 3D landmark of the SLAM algorithm.

III. 3D Navigation Algorithm

A. EKF SLAM for camera-laser sensor based navigation

The proposed indoor navigation algorithm is based on an EKF SLAM algorithm. At the initial stage of this algorithm, depth information received from laser scanner is combined with the bearings of the image features, and then two-dimensional image *features* are transformed to three-dimensional *landmarks* as shown in Fig. 4. Finally the newly acquired landmarks are added to the states of the EKF algorithm.

The goal of the filter is to estimate the states of the vehicle and the landmarks $\mathbf{x}_k=\left[\left(\mathbf{r}\right) \; \left(\mathbf{p}_m^I\right)_1 \; \ldots \; \left(\mathbf{p}_m^I\right)_N\right]^T$ where $\mathbf{r}=\left[\mathbf{p}_R^I \;\; \mathbf{v}_R^I \;\; \Phi_R \;\; \boldsymbol{\omega}\right]$ is position, velocity, attitude and angular velocity of the vehicle, and $\mathbf{p}_m^I$ is the position of the landmark in a static 3D environment.

B. EKF prediction

After the initialization, the 6-DOF pose of the vehicle is predicted by angular rates and accelerations of the IMU with its Gaussian uncertainty. The state vector $\mathbf{x}_{k-1|k-1}$ at step k-1 is propagated to step k through the dynamic model of the vehicle as

$$\hat{\mathbf{x}}_{k|k-1} = \mathbf{f}_k\left(\hat{\mathbf{x}}_{k-1|k-1}, u_k\right). \tag{9}$$

In (9), u_k stands for the control and sensor input at step k. The dynamic model is a nonlinear kinematic model. The covariance matrix is updated at the EKF prediction stage:

$$\mathbf{P}_{k|k-1} = \mathbf{F}_k \mathbf{P}_{k-1|k-1} \mathbf{F}_k^T + \mathbf{G}_k \mathbf{Q}_k \mathbf{G}_k^T \tag{10}$$

where $\mathbf{F}_k$ is the Jacobian matrix, $\mathbf{Q}_k$ is the zero-mean Gaussian noise covariance of the dynamic model, and $\mathbf{G}_k$ is the Jacobian matrix of $\mathbf{Q}_k$ with respect to the vehicle state vector at step k. The state covariance matrix is composed of four sections: robot to robot, robot to landmark, landmark to robot, and landmark to landmark state covariance.

$$\mathbf{P}_k = \begin{bmatrix} \mathbf{P}_{R/R} & \mathbf{P}_{R/m} \\ \mathbf{P}_{R/m} & \mathbf{P}_{m/m} \end{bmatrix} \tag{11}$$

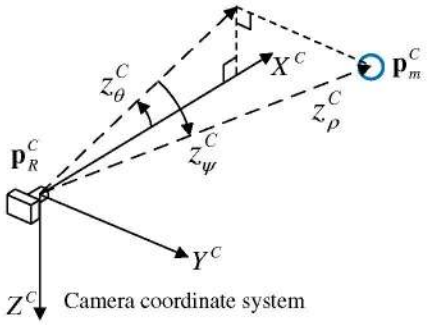

Figure 5. Geometry of a landmark in the camera coordinate system.

C. Measurement Model and Management of Landmarks

The measurement model consists of azimuth, elevation, and range toward the landmark position. The first two components are the relative angle with regard to the principal axis line of the camera, and they can be calculated by attitude and relative position between the camera and the landmark using a pinhole camera model as shown in Fig. 5 and the equation below:

$$\hat{\mathbf{z}}_k = h\left(\mathbf{r}_{k|k-1}, \mathbf{p}_m^C\right) = \begin{bmatrix} \hat{z}_\theta^C \\ \hat{z}_\psi^C \\ \hat{z}_\rho^C \end{bmatrix} = \begin{bmatrix} \tan^{-1}\left(-z_m^C / x_m^C\right) \\ \tan^{-1}\left(y_m^C \Big/ \sqrt{\left(x_m^C\right)^2 + \left(z_m^C\right)^2}\right) \\ \sqrt{\left(x_m^C\right)^2 + \left(y_m^C\right)^2 + \left(z_m^C\right)^2} \end{bmatrix} \tag{12}$$

where $\left\{\hat{z}_\theta^C, \hat{z}_\psi^C, \hat{z}_\rho^C\right\}$ are elevation, azimuth and range in the camera coordinate system, respectively.

Three measurements are acquired by the camera and the laser scanner directly. However, the laser scanner does not provide range for all landmarks in a given time step because only a few features are located in the intersection of a laser scan plane and the line of sight towards a landmark in an image from the camera. Therefore, most landmarks, which are not located in a camera-laser intersection, use only the first two measurements, elevation and azimuth, in (12).

The position of features and landmarks in the image coordinates are tracked as explained in the previous section. If landmarks move out of the field of view of the camera, then they are removed from the filter states and covariance matrix since they can no longer be tracked in the successive images.

New landmarks registered for the first time are added to the states and covariance of the filter at the end of the filter loop. A new landmark is initialized when the line of sight towards a feature in the camera's view and the scan plane of the laser scanner intersect for the first time. The new landmark also inherits initial covariance matrix values.

D. EKF correction

At the EKF correction stage, measured data from the laser scanner and the camera correct all states and covariance of the vehicle and the landmarks. A measurement data form for a given landmark has either two values {elevation, azimuth} or three values {elevation, azimuth, range}, as explained previously.

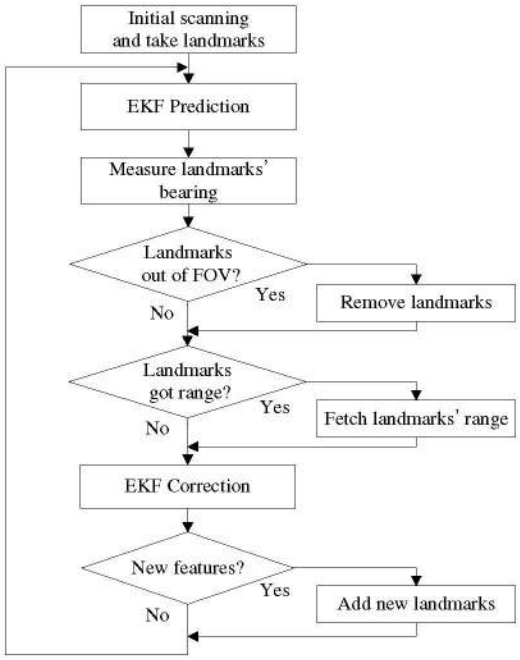

Figure 6. Flow chart of the proposed navigation algorithm.

Assuming that the measurement of a landmark is not coupled with the other landmarks, but is only coupled with position and attitude of the vehicle, we can divide the measurements and the Jacobian matrix $\mathbf{H}_{k,[i]}$ for each *i-th* landmark

$$\mathbf{H}_{k,[i]} = \frac{\partial h\left(\mathbf{r}_{k|k-1}, \mathbf{p}_{m[i]}^C\right)}{\partial \mathbf{x}_k} \tag{13}$$

where $\mathbf{p}_{m[i]}^C$ is the 3-DOF position of the landmark in the camera coordinate system. We can also compute the sensitivity matrix $\mathbf{S}_{k,[i]}$ and the Kalman gain $\mathbf{K}_{k,[i]}$ for each *i-th* landmark

$$\mathbf{S}_{k,[i]} = \mathbf{H}_{k,[i]} \mathbf{P}_{k|k-1} \mathbf{H}_{k,[i]}^T + R_{[i]} \tag{14}$$

$$\mathbf{K}_{k,[i]} = \mathbf{P}_{k|k-1} \mathbf{H}_{k,[i]}^T \left(\mathbf{S}_{k,[i]}\right)^{-1} \tag{15}$$

where $R_{[i]}$ is the Gaussian noise covariance matrix of the sensor for each measurement. The size of the noise covariance matrix depends on the existence of the laser range measurement at the landmark. The computed Kalman gain is multiplied by the innovation of the actual measurement versus the estimated measurement to determine the states and covariance of the vehicle and the landmarks:

$$\hat{\mathbf{x}}_{k|k} = \hat{\mathbf{x}}_{k|k-1} + \mathbf{K}_k \left\{\mathbf{z}_{[i]} - \mathbf{H}_{k,[i]} \hat{\mathbf{x}}_{k|k-1}\right\} \tag{16}$$

$$\mathbf{P}_{k|k} = \left(\mathbf{I} - \mathbf{K}_k \mathbf{H}_k\right) \mathbf{P}_{k|k-1} \,. \tag{17}$$

The flow chart of the proposed camera-laser EKF SLAM algorithm is shown in Fig. 6.

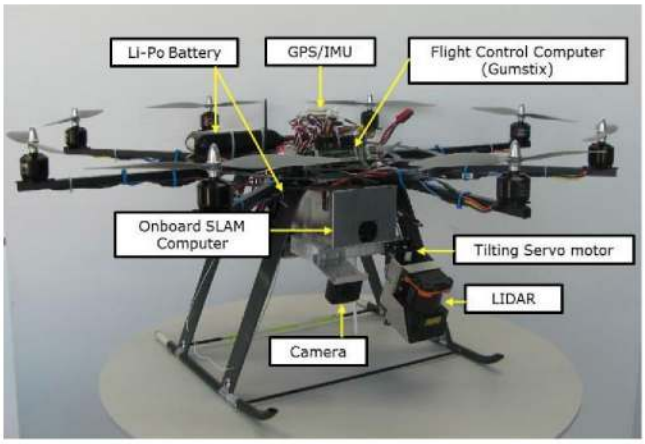

Figure 7. Our octo-rotor UAV platform.

IV. EXPERIMENT

A. Experiment setup

To validate the proposed indoor navigation algorithm, an onboard vision processing computer (Pico-ITX form factor Dual 1.0GHz CPU), a low-level flight controller (Gumstix verdex pro™), a camera-gimbaled laser sensor module (Point Grey FireFly®MV camera, Hokuyo UTM-30LX laser scanner, and Dynamixel MX-28 servo motor), and a GPS-IMU (u-blox 5 and MicroStrain 3DM-GX3®-25) are integrated as an onboard navigation package. The weight of this navigation package is about 1.3kg. Therefore, the octo-rotor aerial vehicle was specifically designed to lift this payload as shown in Fig. 8. The octo-rotor platform has 80cm of motor-to-motor diameter, 6.0kg of total weight, and 15 minutes flight time with Li-Po batteries.

Our system architecture is developed for integrating the camera-gimbaled laser sensor module, the GPS, the low-level flight controller, and an occupancy grid mapper as described in Fig. 7. The low-level flight controller can choose the proper navigation source between the GPS and the camera-laser navigation solution when the system is working outdoors. The attitude and position is controlled by a multi-loop PD controller and the guidance algorithm to follow waypoints or paths is also enabled.

The estimated pose of the vehicle is used for dense 3D grid mapping of the environment around the vehicle so that the vehicle can use the grid map to make feasible path decisions, allowing the vehicle to move around and avoid obstacles in the map. However, the occupancy grid mapping for a 3D environment demands computational load that is too strenuous for the light-weight onboard processor even if an octree structure is used. Therefore, the ground station is inevitably required to download data from the vehicle, process the computations, and upload the computation results to the vehicle.

Communication with the vehicle for monitoring onboard status is performed via Wi-Fi network. All computer vision algorithm development is done in C/C++ using OpenCV library [14].

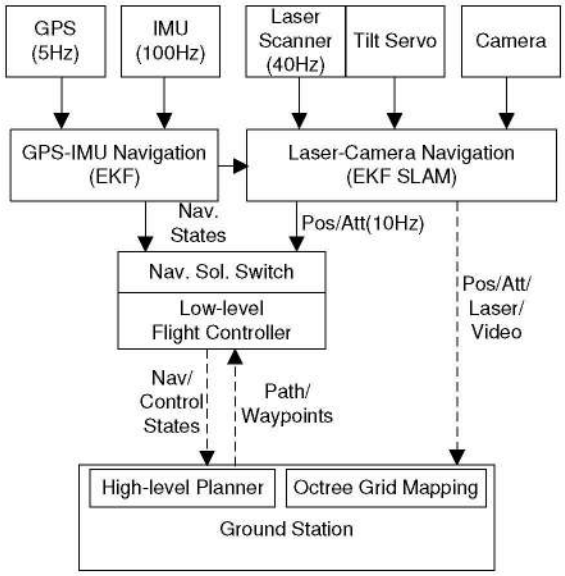

Figure 8. Architecture diagram of our GPS-IMU and camera-laser integrated navigation system.

B. Experiment Result

The algorithm proposed in this paper was applied to onboard video and data taken from the vehicle. The indoor experiment video and data shown in Fig. 9 were captured by a hand-held test in a space measuring roughly 11 m × 7 m. A point cloud map and an octree-based occupancy grid map were generated using the estimated navigation solution.

While we did not have access to ground truth trajectory of the vehicle, we were able to test our algorithms on real test data. The accuracy of our states can be validated qualitatively by looking at the accurate reconstruction of the 3D

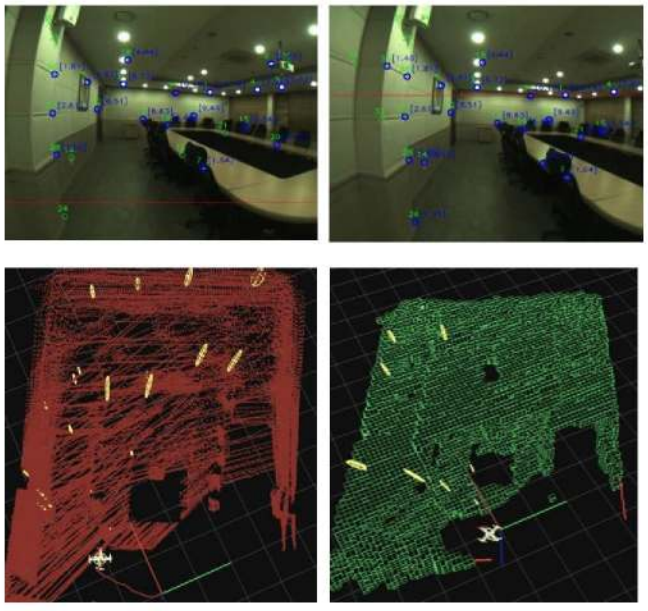

Figure 9. (a-b) Pictures of the indoor space where the navigation algorithm was tested. The numbers and circles stand for landmarks, and the sensor module was moved by hand. (c) 3D visualization of proposed camera-laser navigation result: Point clouds are rendered using the estimated states. (d) Occupancy grid map using the estimated states.

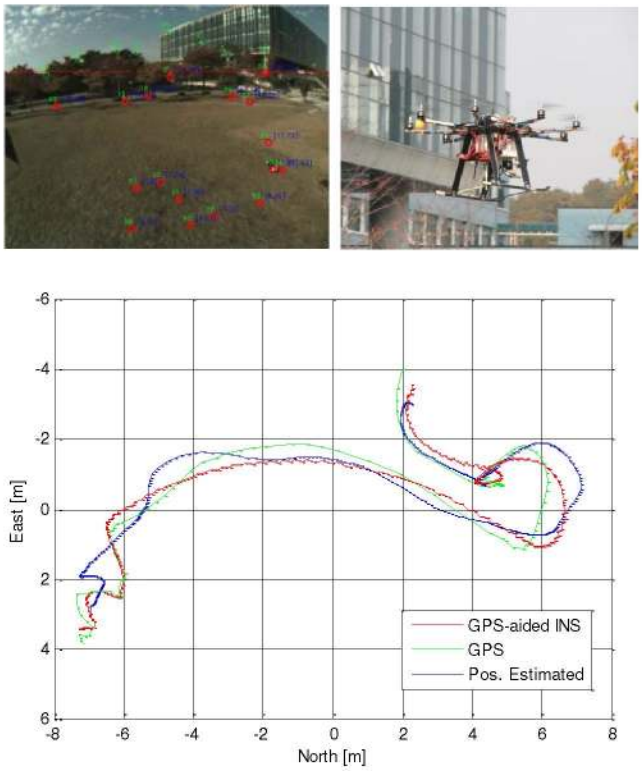

Figure 10. Pictures of the outdoor space and the octo-rotor UAV (top). The graph represents the estimated vehicle trajectory and GPS positions (bottom)

environment by reprojection of the laser scanned points using estimated vehicle states. One such 3D point cloud and grid map is shown in Fig. 9.

The outdoor experiment video and data shown in Fig. 10 were captured by the onboard computer, and the proposed camera-laser navigation algorithm was applied. The estimated states were validated quantitatively by comparing the estimated trajectory with that of GPS which showed an accuracy of less than 1 meter, even in the wide open space which exceeds the laser range. There are fewer usable features within view of the camera than in indoor environments since the features are located farther away than the range of the laser. Our camera is looking downward at a 10 degree pitch, but a more downward pitching angle is desirable for better feature extraction and tracking.

There is almost no vibration that disturbs the data acquisition from the camera and the laser on the gimbaled servo. However, fast maneuvers can easily cause the feature tracking to fail. There needs to be a tighter integration method between the camera and the IMU in order to improve the feature tracking ability.

V. Conclusion

In this paper, we presented a navigation system that integrates a camera, a gimbaled laser scanner and an IMU for unmanned vehicles to move autonomously in both indoor and outdoor environments. Our onboard navigation system can provide a real-time, 3D navigation solution without any pre-assumptions.

We proposed a camera and gimbaled laser sensor calibration method to calculate the relative pose between them. In addition, we presented a real-time navigation algorithm based on an online EKF SLAM algorithm. We demonstrated the performance of our system in indoor and outdoor environments. The experimental results clearly showed the advantages of our navigation system.

Future work will include improvements to the navigation algorithm to make it more robust so that it can cope with various dynamic environments. In addition, the state estimation and control algorithms will be integrated to perform closed-loop flights, both indoors and outdoors.

References

[1] A. Bachrach, S. Prentice, R. He and N. Roy, "RANGE—Robust Autonomous Navigation in GPS-Denied Environments," *Journal of Field Robotics,* vol. 28, no. 5, pp. 644-666, 2011.

[2] S. Grzonka, G. Grisetti and W. Burgard, "A Fully Autonomous Indoor Quadrotor," *IEEE Transactions on Robotics,* vol. 28, no. 1, pp. 90-100, 2012.

[3] S. Shen, N. Michael and V. Kumar, "Autonomous multi-floor indoor navigation with a computationally constrainted mav," in *Proc. of the IEEE Int. Conf. on Robotics and Automation (ICRA)*, 2011.

[4] F. Fraundorfer, L. Heng, D. Honegger, G. H. Lee, L. Meier, P. Tanskanen and M. Pollefeys, "Vision-Based Autonomous Mapping and Exploration Using a Quadrotor MAV," in *Proc. of the IEEE Int. Conf. on Intelligent Robots and Systems (IROS)*, 2012.

[5] A. Bachrach, S. Prentice, R. He, P. Henry, A. S. Huang, M. Krainin, D. Maturana, D. Fox and N. Roy, "Estimation, planning, and mapping for autonomous flight using an RGB-D camera in GPS-denied environments," *The International Journal of Robotics Research,* vol. 31, no. 11, pp. 1320-1343, 2012.

[6] M. Achtelik, M. Achtelik, S. Weiss and R. Siegwart, "Onboard IMU and monocular vision based control for MAVs in unknown in- and outdoor environments," in *Proc. of the IEEE Int. Conf. on Robotics and Automation (ICRA)*, Shanghai, China, 2011.

[7] S. Weiss, D. Scaramuzza and R. Siegwart, "Monocular-SLAM–Based Navigation for Autonomous Micro Helicopters in GPS-Denied Environments," *Journal of Field Robotics,* vol. 28, no. 6, pp. 854-874, 2011.

[8] A. Bry, A. Bachrach and N. Roy, "State Estimation for Aggressive Flight in GPS-Denied Environments Using Onboard Sensing," in *Proc. of the IEEE Int. Conf. on Robotics and Automation (ICRA)*, 2012.

[9] J. Civera, A. J. Davison and J. M. M. Montiel, "Inverse Depth Parametrization for Monocular SLAM," *IEEE Transactions on Robotics,* vol. 24, no. 5, pp. 932-945, 2008.

[10] R. Unnikrishnan and M. Hebert, "Fast Extrinsic Calibration of a Laser Rangefinder to a Camera," Tech. Report CMU-RI-TR-05-09, Robotics Institute, Carnegie Mellon University, July, 2005.

[11] R. Hartley and A. Zisserman, Multiple View Geometry in Computer Vision, Cambridge, 2000.

[12] E. Rosten and T. Drummond, "Machine Learning for High-Speed Corner Detection," in *Proc. of European Conference on Computer Vision (ECCV)*, 2006.

[13] J. Shi and C. Tomasi, "Good Features to Track," in *Proc. of Computer Vision and Pattern Recognition (CVPR)*, 1994.

[14] J.y. Bouguet, "Pyramidal implementation of the Lucas Kanade feature tracker," *Intel Corporation, Microprocessor Research Labs,* 2000.

[15] "OpenCV (Open Source Computer Vision Library)," [Online]. Available: http://opencv.org/.